

Turbulence Dynamics In Irregular Breaking Waves

Francis C. K. Ting

Department of Civil and Environmental Engineering

South Dakota State University

Brookings, SD 57007

phone: (605) 688-5997 fax: (605) 688-5878 email: Francis_Ting@sdstate.edu

Award Number: N00014-00-1-0461

<http://www.engineering.sdstate.edu/~fluidlab>

LONG-TERM GOALS

Our long-term goals are to provide a detailed picture of the breaking and decay of irregular waves in a laboratory surf zone, and of the generation and evolution of the related turbulent flow fields.

OBJECTIVES

Our current work focuses on measurement of the temporal and spatial distributions of wave-induced stresses and turbulent stresses under regular and irregular waves on a plane beach using a two-component laser Doppler anemometer (LDA), and measurement of coherent structures under breaking waves using a stereoscopic particle image (PIV) velocimetry system.

APPROACH

Laboratory experiments were conducted in a 25 m long, 0.9 m wide and 0.75 m deep precision tilting flume equipped with a programmable random wave generator. A constant slope of 1 in 50 was used in all the experiments. Irregular waves were produced using the JONSWAP wave spectrum. The regular waves were cnoidal waves. Two resistance-type wave gages mounted on an instrument carriage was positioned sequentially at 11 locations (22 wave gage locations) inside the surf zone to measure the wave transformation. A video camera recorded the surface waves at each carriage location. The video recordings were synchronized with the wave measurements to determine the temporal and spatial distributions of wave breaking, and the breaker types.

In the inner surf zone, the velocity components parallel to the slope, u , and normal to the slope, w , were measured in a vertical line from the wave trough level to approximately 2.0 mm above the flume bottom using a two-component LDA. For irregular waves, the duration of wave measurements was 10 minutes. Water particle velocities were measured 14 times at each elevation, with the same incident wave time series. For regular waves, at least 110 wave cycles were measured at each elevation. The measured instantaneous velocities were separated into a deterministic (wave) component and a random (turbulence) component by ensemble averaging, that is, $(u, w) = (\langle u \rangle + u', w = \langle w \rangle + w')$, where the operator $\langle \rangle$ denotes ensemble averaging, and the tilde denotes turbulent fluctuation.

The instantaneous velocity field under a breaking solitary wave was measured in a horizontal plane close to the flume bed using a stereoscopic PIV system. A total of 27 test runs were completed under the same experimental conditions. In each test run, 215 instantaneous velocity vector fields were

captured at a sampling interval of 1/15 s. The organized wave-induced velocity was found by computing at each time step and at each node the mean of the velocity vectors from all 27 test runs. The resulting ensemble-averaged velocity fields were subtracted from the individual measured velocity fields to obtain the instantaneous turbulent velocity fields.

WORK COMPLETED

The wave measurements and the LDA measurements described above were completed for two different irregular wave conditions and three different regular wave conditions. In addition to the wave statistics for the 10-minute time series, two representative wave groups from the irregular wave trains were selected to do a complete wave-by-wave analysis, by following the propagation of the individual waves through the surf zone (Louwagie, 2003; Peterson, 2003). Information extracted from the wave groups includes the transformation of wave height, wave period, wave length, wave celerity, and four wave shape parameters (wave steepness, wave crest front steepness, horizontal symmetry and vertical symmetry). The results from irregular waves were compared with similar results from regular waves. The wave-induced stresses $\langle u \rangle^2$, $\langle w \rangle^2$, $\langle u \rangle \langle w \rangle$; and the Reynolds stresses $\langle u'^2 \rangle$, $\langle w'^2 \rangle$, $\langle u'w' \rangle$ were calculated from the velocity measurements. The data were examined to determine the contributions of wave velocity and turbulence velocity to the total stresses. Also studied were the instantaneous Reynolds stresses u'^2 , w'^2 and $u'w'$. Conditional averaging methods were used to obtain the statistics of coherence turbulence and their distributions over the water column.

RESULTS

Figure 1 shows the vertical distributions of the time-mean values of the wave-induced shear stress $\langle u \rangle \langle w \rangle$, Reynolds normal stresses $\langle u'^2 \rangle$, $\langle w'^2 \rangle$, and Reynolds shear stress $\langle u'w' \rangle$ under two different irregular wave conditions. Figure 2 shows the vertical distributions of the time-mean stresses in a spilling regular wave for comparison purposes. The vertical coordinate, z , is measured from the still water surface. When averaged over time, the turbulent kinetic energy defined by $(\langle u'^2 \rangle + \langle w'^2 \rangle)/2$ is considerably larger in regular waves than in irregular waves near the free surface. Close to the bottom, the regular waves and the irregular waves have about the same time-mean turbulent kinetic energy values. In both regular and irregular waves, the Reynolds shear stress $\langle u'w' \rangle$ is larger than the wave-induced shear stress $\langle u \rangle \langle w \rangle$ near the free surface, but smaller than the wave-induced shear stress near the bottom. In the regular waves, $\langle u \rangle$ and $\langle w \rangle$ include the undertow and a periodic wave component. In the irregular waves, there is an additional contribution from the orbital velocity of the low-frequency waves (surf beat). The latter was found to be a significant fraction of the total velocity.

Figure 3 shows the time histories of wave-induced horizontal velocity $\langle u \rangle$, wave-induced shear stress $\langle u \rangle \langle w \rangle$, and ensemble-averaged Reynolds shear stress $\langle u'w' \rangle$ under an irregular breaking wave. Also shown are the time histories of the instantaneous Reynolds shear stress $u'w'$ from two different test runs conducted under the same experimental conditions (the same experiment was repeated 14 times). These measurements were taken at a height of 2.5 mm above the flume bed. As seen, the ensemble-averaged Reynolds shear stress $\langle u'w' \rangle$ is several times smaller than the wave-induced shear stress $\langle u \rangle \langle w \rangle$. However, the instantaneous Reynolds shear stress $u'w'$ is of the same order of magnitude as the wave-induced shear stress $\langle u \rangle \langle w \rangle$. Inspection of the time series of $u'w'$ revealed that in the upper half of the water column, the instantaneous Reynolds shear stress

appears in well-defined turbulent bursts. Furthermore, most of the bursts have negative $u'w'$ values. Near the bottom, there are many more turbulence bursts. However, the bursts are much shorter, and there are as many positive bursts as negative bursts (see test 6 and test 8 in Figure 3).

Nadaoka et al. (1989) observed that the wave breaking process produces horizontal vortices in the span-wise direction, which then rapidly break down through the formation of vortices extending obliquely downward. Using a conditional sampling technique, Nadaoka et al. (1988) showed that intense, intermittent turbulence transports large amount of turbulent kinetic energy and fluid momentum to the bottom. More recently, Cox and Kobayashi (2000) showed that intermittent turbulence penetrates the bottom boundary layer for spilling regular waves, and produces turbulent kinetic energy and Reynolds stress that are an order of magnitude larger than the phase-averaged values. They also showed that intermittent turbulent motions account for a significant fraction of the total turbulent kinetic energy and Reynolds stress in the entire time series.

A computer program was written to calculate the statistics of turbulence bursts defined by the Reynolds shear stress. A burst is detected when the value of $u'w'$ becomes negative. The program computes the height and period of the individual bursts defined by their zero-crossing points. The bursts are then counted and arranged in descending order of burst height, until one-tenth of the total number of bursts is reached. The means of the burst heights and periods are calculated and termed the height and period of the highest one-tenth burst. Their variations with the vertical coordinate are plotted in Figure 4 for spilling regular waves. Also plotted is the amplitude of the wave-induced shear stress $\langle u \rangle \langle w \rangle$. As shown in Figure 4, the burst height is comparable to the amplitude of the wave-induced shear stress throughout the water column. The burst period increases with distance from the still water surface in the upper half of the water column and then decreases. The large amplitudes (relative to $\langle u \rangle \langle w \rangle$) and long durations (relative to the wave period) of the turbulence bursts suggest that these intermittent turbulent events may be dynamically significant. Furthermore, the variation of burst period with depth suggests well-organized turbulent flow structures near the water surface but less coherent turbulence near the bottom, consistent with break-down of large eddies outside the region affected by the surface roller.

IMPACT/APPLICATIONS

Understanding the distributions of wave-induced stresses and turbulence stresses in breaking waves is important to the development of improved parameterizations of wave breaking effects in the surf zone. The structure of coherent turbulence is important to sediment suspension on beaches.

RELATED PROJECTS

NSF Grant Number CTS-0078926, "Acquisition of a Multi-Purpose Open-Channel Flume for Water Flow Studies," Francis C. K. Ting et al., South Dakota State University. This equipment grant has provided partial funding for the flume.

N00014-99-1-1051 (NOPP), "Development and Verification of a Comprehensive Community Model for Physical Processes in the Nearshore Ocean," James T. Kirby et al., University of Delaware. We have provided velocity measurements to Ib Svendsen for comparison with numerical model predictions.

REFERENCES

- Cox, D. T. and Kobayashi, N. (2000). "Identification of intense, intermittent coherent motions under shoaling and breaking waves," *Journal of Geophysical Research*, Vol. 105, No. C6, pp. 14,223-14,236.
- Nadaoka, K., Hino, M. and Koyano, Y. (1989). "Structure of the turbulent flow field under breaking waves in the surf zone," *Journal of Fluid Mechanics*, Vol. 204, pp. 359-387.
- Nadaoka, K., Ueno, S. and Igarashi, T. (1988). "Sediment suspension due to large scale eddies in the surf zone," *Proceedings of the 21st International Coastal Engineering Conference*, Torremolinos, Spain, ASCE, New York, pp. 1,646-1660.

PUBLICATIONS

- Louwagie, R. A. (2003). *Transformation of irregular wave groups in a laboratory surf zone*, M.S. Thesis, Department of Civil and Environmental Engineering, South Dakota State University, Brookings, South Dakota, published.
- Peterson, E. J. (2003). *Transformation of irregular breaking waves in a laboratory surf zone*, M.S. Thesis, Department of Civil and Environmental Engineering, South Dakota State University, Brookings, South Dakota, submitted.

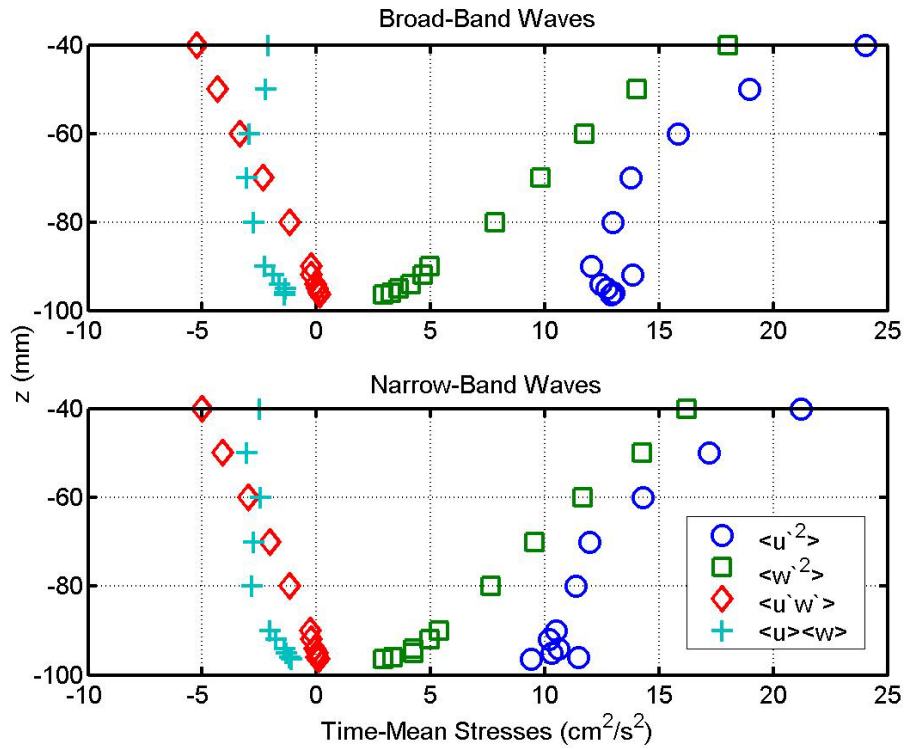


Figure 1. Vertical distributions of turbulent and wave-induced stresses under irregular waves. The local significant wave height and wave period are 0.063 m and 1.64 s for the broad band waves; and 0.064 m and 1.71 s for the narrow band waves. The local still water depth is 98.5 mm.

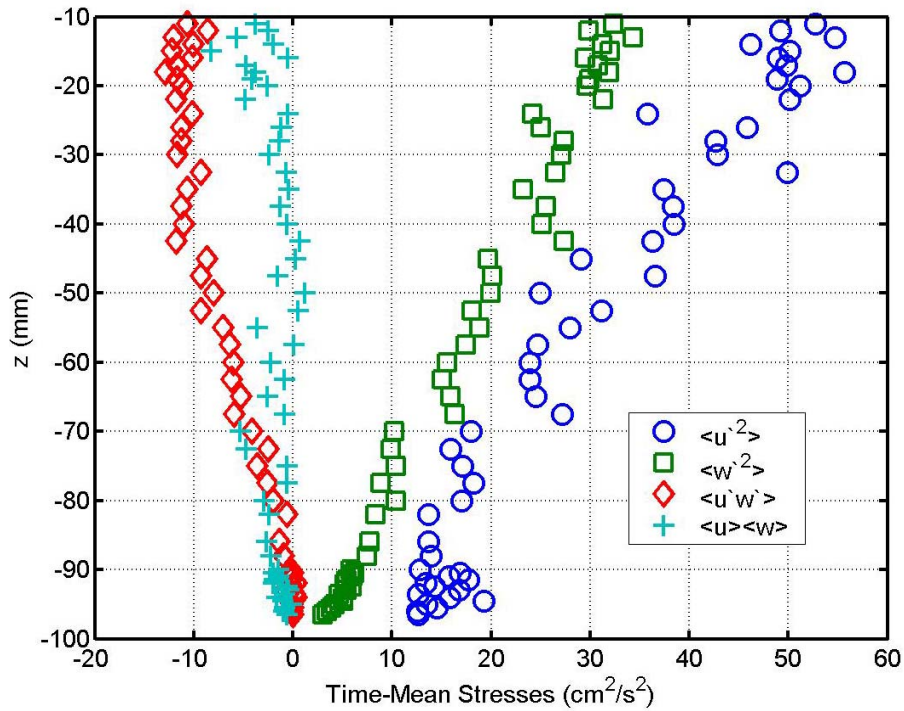


Figure 2. Vertical distributions of turbulent and wave-induced stresses under spilling regular waves. The wave period is 1.8 s, and the wave height is 0.048 m. The local still water depth is 98.5 mm.

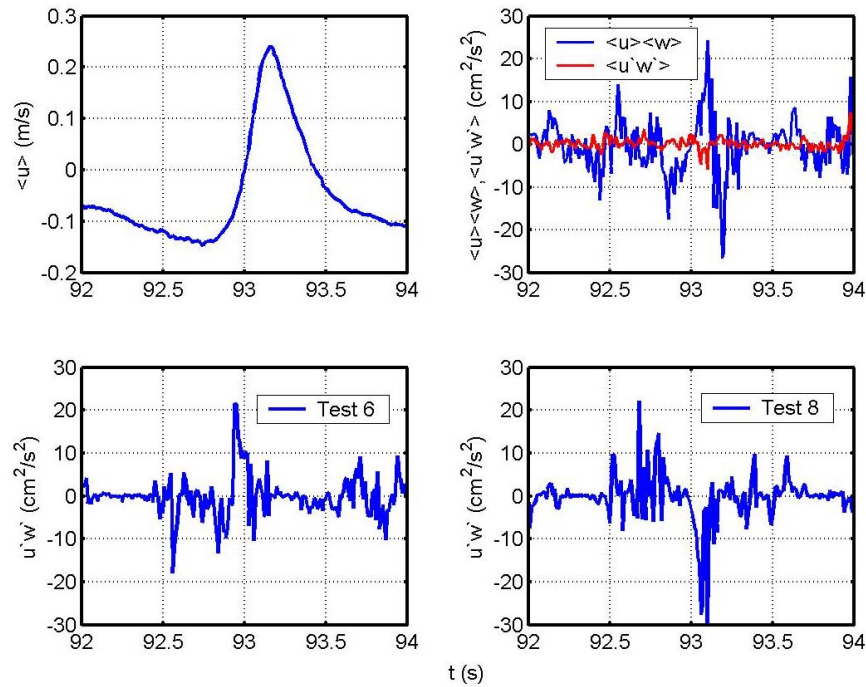


Figure 3. Time histories of wave-induced velocity $\langle u \rangle$, wave-induced shear stress $\langle u \rangle \langle w \rangle$, and ensemble-averaged Reynolds shear stress $\langle u'w' \rangle$ under an irregular breaking wave. The two lower plots show the instantaneous Reynolds shear stress $u'w'$ from two different tests (6 and 8) with the same experimental conditions.

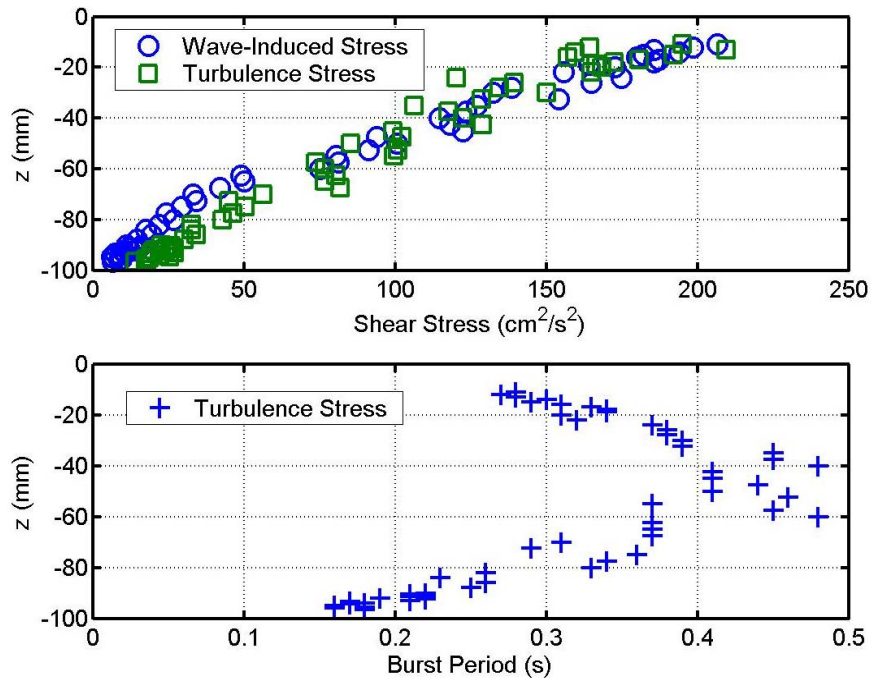


Figure 4. Vertical distributions of amplitude of wave-induced shear stress $\langle u \rangle \langle w \rangle$, and height (upper plot) and period (lower plot) of the highest one-tenth turbulent burst defined by the instantaneous Reynolds shear stress $u'w'$. The experimental data are for spilling regular waves.